Time-dependent perturbation theory beyond the dipole approximation for two-photon ionization of atoms

Mu-Xue Wang,[1] Hao Liang,[1] Xiang-Ru Xiao,[1] Si-Ge Chen,[1] and Liang-You Peng[1,2,3,*]

[1]*State Key Laboratory for Mesoscopic Physics and Collaborative Innovation Center of Quantum Matter, School of Physics, Peking University, Beijing 100871, China*

[2]*Beijing Academy of Quantum Information Sciences, Beijing 100193, China*

[3]*Collaborative Innovation Center of Extreme Optics, Shanxi University, Taiyuan, Shanxi 030006, China*

(Received 21 December 2018; published 5 February 2019)

We develop a time-dependent perturbation theory (PT) beyond the dipole approximation to analyze the two-photon ionization dynamics of atoms exposed to short laser pulses with an arbitrary polarization. In a wide range of laser parameters, the good performance of the PT method is validated by comparing the results of a number of physical quantities with those calculated by numerically solving the time-dependent Schrödinger equation beyond the dipole approximation. Subsequent applications of the PT method in the nonresonant regime allow us to unveil the important role of the interferences between the dipole and nondipole transition pathways to the photoelectron momentum shift along the laser-propagation direction. In particular, we find that the ratio of the probability of each dipole transition channel to the total ionization probability oscillates with the increase of the photon energy. The interferences among different pathways and the oscillatory behavior of the ratios jointly lead to a series of minima in the linear momentum transfer for the case of the linear polarization.

DOI: 10.1103/PhysRevA.99.023407

I. INTRODUCTION

Rapid advances in free-electron lasers (FELs) [1–3] make it possible to produce x rays at wavelengths down to 1 Å with an unprecedented intensity around 10^{20} W/cm^2 (see, e.g, a recent review in Ref. [4] and references therein). The availability of these new light sources has provided opportunities to investigate nonlinear processes in the short-wavelength regime. To achieve a fundamental understanding of nonlinear processes, the multiphoton ionization of atoms has garnered a lot of attention for decades [5–12]. As the simplest multiphoton process, a number of alternative approaches have been reported for the cases when at least two photons are necessary to reach the continuum [13–17] and the cases of two-photon above-threshold ionization [18–21]. The total cross sections and angular distributions of electrons emitted in the two-photon ionization processes have been discussed both within and beyond the dipole approximation [22–26]. Theories of two-photon double ionization have also been reported [27–29]. In the case of few-cycle short XUV laser pulses, the carrier envelope phase effects [30] originated from the interference of the first- and second-order transition amplitudes have been treated perturbatively [31,32]. Studies have also been carried out on the circular or elliptic dichroism in the two-photon process by an elliptically polarized monochromatic laser field [33,34].

In the dipole approximation, the time-dependent Hamiltonian has a cylindrical symmetry for a linearly polarized laser pulse. However, the inclusion of the leading-order correction beyond the dipole approximation into the Hamiltonian [35–37] will break this symmetry and bring about prominent nondipole effects, which have recently attracted great attention in the study of high-harmonic generation [38], atomic stabilization [39,40], double ionization [41,42], and dynamic interference [43]. A unique nondipole lobe has been theoretically predicted [44] along the laser-propagation direction in the angular distribution of $H(1s)$ in a super-intense and high-frequency pulse. In some cases, the interferences between the dipole ionization paths and the nondipole ionization paths can lead to asymmetrical angular distributions [45,46] and nondipole contributions to the photoelectron spin polarization have been discussed [47]. The retardation effects in two-photon processes of stimulated Compton scattering and stimulated Raman scattering have also been discussed in detail [48,49]. Another hot topic of the nondipole effects is the photon-momentum transfer and partition in atomic and molecular ionization [50–57]. In this case, the linear momentum of the photon is related to the average value of the photoelectron momentum along the laser propagation direction, whose nonzero value is a manifestation of the nondipole effects.

In a previous work, we have provided detailed *ab initio* simulations of photon-momentum-transfer rules in the region of few-photon ionization [56]. In the present work, we develop a time-dependent perturbation theory (PT) beyond the dipole approximation to treat the two-photon ionization of atoms. Specifically, we investigate the two-photon ionization of the hydrogen atomic system exposed to a laser pulse with a central frequency ranging from 0.28 to 0.48 a.u. and with a pulse duration varying from 0.87 to 20 fs. Applied in the region off a resonance, the accurate perturbative analysis allows us to reveal the underlying mechanisms of the nondipole effects for the two-photon ionization of the hydrogen ground state.

*liangyou.peng@pku.edu.cn

The rest of the paper is organized as follows. In Sec. II, we present the second-order PT method beyond the dipole approximation. In Sec. III A, its performance is verified by comparing the photoelectron energy distributions, ionization probabilities, and nondipole angular distributions, with those calculated from the numerical solution to the time-dependent Schrödinger equation. We show that the PT method works well even for an ultrashort few-cycle laser pulse in the cases where resonance frequency components do not play an important role in the broad bandwidth of the short pulse. In Sec. III B, we apply the PT method in the nonresonant regime to analyze one of the most important nondipole effects, i.e., the linear-momentum-transfer law in the two-photon ionization process. We identify the reasons for the minima in the momentum shift for the case of a linear polarization, i.e., they originate from the interferences among the dipole and nondipole ionization paths, and the oscillation behavior of the ratios of the ionization probabilities through different dipole paths to the total ionization probability. Atomic units (a.u.) are used throughout this paper unless explicitly specified otherwise.

II. TIME-DEPENDENT PERTURBATION METHOD

With the inclusion of the lowest-order corrections beyond the dipole approximation to the Hamiltonian, the dynamics of a hydrogen atom interacting with a laser pulse is described by the time-dependent Schrödinger equation (TDSE) [43,56]

$$i\frac{\partial}{\partial t}\Psi(\mathbf{r},t)=[H_0+H_I(t)]\Psi(\mathbf{r},t), \tag{1}$$

where in the velocity gauge,

$$H_0=\frac{\mathbf{p}^2}{2}+V(r)=\frac{\mathbf{p}^2}{2}-\frac{1}{r}, \tag{2}$$

$$H_I(t)=\mathbf{p}\cdot\mathbf{A}(t)+\frac{z}{c}\mathbf{p}\cdot\mathbf{E}(t)+\frac{z}{c}\mathbf{A}(t)\cdot\mathbf{E}(t), \tag{3}$$

in which the momentum operator $\mathbf{p}=-i\nabla$, and $\mathbf{A}(t)$ and $\mathbf{E}(t)$ are the vector potential and electric field for the laser pulse under the usual dipole approximation.

Due to the spherical symmetry of the Coulomb potential, the electron wave function can be expanded in terms of the spherical harmonics. In this work, we consider the two-photon ionization from the hydrogen ground state

$$\Psi_i(\mathbf{r})=2e^{-r}Y_{00}(\hat{\mathbf{r}}), \tag{4}$$

to a final continuum state [58]

$$\Psi_{\mathbf{p}}^{(-)}(\mathbf{r})=\frac{1}{\sqrt{2\pi}\,p}\sum_{l,m}i^l\,e^{-i(\sigma_l+\delta_l)}Y_{lm}^*(\hat{\mathbf{p}})R_{pl}(r)Y_{lm}(\hat{\mathbf{r}}), \tag{5}$$

in which $\mathbf{p}=(p,\hat{\mathbf{p}})=(p,\theta,\phi)$.

Without the loss of generality, we consider a short laser pulse with an arbitrary polarization with an ellipticity η. In particular, $\eta=0$ for the linear polarization and $\eta=1$ for the right-handed circular polarization. We assume that an N-cycle laser with a central frequency ω_0 propagates along the positive z axis, and the component of the vector potential in the dipole approximation is given by

$$\mathbf{A}(t)=\frac{A_0}{\sqrt{1+\eta^2}}\cos^2\left(\frac{\omega_0 t}{2N}\right)[\cos(\omega_0 t)\mathbf{e}_x+\eta\sin(\omega_0 t)\mathbf{e}_y],$$

and its Fourier transform is defined as $\hat{\mathbf{A}}(\omega)$, i.e.,

$$\hat{\mathbf{A}}(\omega)=\int_{t_i}^{t_f}\mathbf{A}(t)e^{i\omega t}\,dt. \tag{6}$$

The corresponding electric field is $\mathbf{E}(t)=-\partial\mathbf{A}(t)/\partial t$ with its Fourier transform $\hat{\mathbf{E}}(\omega)$ given by

$$\hat{\mathbf{E}}(\omega)=\int_{t_i}^{t_f}\mathbf{E}(t)e^{i\omega t}\,dt. \tag{7}$$

According to the second-order perturbation theory, by using similar derivations with those presented in Refs. [31,32] for the dipole case, it is easy to obtain the expression of the two-photon transition amplitude from the initial state $\Psi_i(\mathbf{r})$ to the final state $\Psi_{\mathbf{p}}^{(-)}(\mathbf{r})$ for the nondipole interaction Hamiltonian $H_I(t)$ in Eq. (3). The resultant amplitude is given by

$$\begin{aligned}A_2(\mathbf{p})=\langle\Psi_{\mathbf{p}}^{(-)}|-\frac{1}{2\pi}\int d\varepsilon\left[\mathbf{p}\cdot\hat{\mathbf{A}}(E_f-\varepsilon)+\frac{z}{c}\mathbf{p}\cdot\hat{\mathbf{E}}(E_f-\varepsilon)\right]\\ \times G_\varepsilon(\mathbf{r},\mathbf{r}')\left[\mathbf{p}\cdot\hat{\mathbf{A}}(\varepsilon-E_i)+\frac{z'}{c}\mathbf{p}\cdot\hat{\mathbf{E}}(\varepsilon-E_i)\right]\\ +\frac{z}{c}\hat{F}(E_f-E_i)|\Psi_i\rangle,\end{aligned} \tag{8}$$

where E_i is the ground-state energy and $E_f=p^2/2$ is the final kinetic energy, and we define $\hat{F}(E_f-E_i)$ to be

$$\hat{F}(E_f-E_i)=\int_{t_i}^{t_f}\mathbf{A}(t)\cdot\mathbf{E}(t)\,e^{i(E_f-E_i)t}\,dt. \tag{9}$$

In Eq. (8), the Coulomb Green's function (CGF) for the electron [59–61]

$$G_\varepsilon(\mathbf{r},\mathbf{r}')=\sum_{klm}\frac{|\Psi_{klm}\rangle\langle\Psi_{klm}|}{E_k-\varepsilon}+\int d\mathbf{p}\frac{|\Psi_{\mathbf{p}}^{(-)}\rangle\langle\Psi_{\mathbf{p}}^{(-)}|}{p^2/2-\varepsilon-i0} \tag{10}$$

can be expanded through the spherical harmonics, i.e.,

$$G_\varepsilon(\mathbf{r},\mathbf{r}')=\sum_{lm}g_l(\varepsilon;r,r')Y_{lm}(\hat{\mathbf{r}})Y_{lm}^*(\hat{\mathbf{r}}'), \tag{11}$$

in which the radial part $g_l(\varepsilon;r,r')$ can be expanded into series in Sturm's function of the Coulomb problem and the result rapidly converges for a negative value of the virtual intermediate state's energy ε [61].

With the above formulation, the two-photon transition amplitude $A_2(\mathbf{p})$ given by Eq. (8) can now be numerically evaluated. For the purpose of the present work to investigate the photon momentum transfer along the z axis, one needs to extract the photoelectron momentum along the laser propagation direction. For convenience, the three-dimensional photoelectron momentum distribution

$$P(\mathbf{p})=P(p,\theta,\phi)=|A_2(\mathbf{p})|^2 \tag{12}$$

is changed from the spherical coordinates (p,θ,ϕ) to the cylindrical coordinates (p_ρ,p_z,ϕ) with a very high accuracy through the method of Gouraud shading [62]. Then, the

electron momentum distribution along the laser propagation direction can be calculated by

$$f(p_z) = \iint P(p_\rho, p_z, \phi) p_\rho \, dp_\rho \, d\phi, \tag{13}$$

from which one can evaluate the electron average momentum $\langle p_z \rangle$ as follows:

$$\langle p_z \rangle = \frac{\int p_z f(p_z) dp_z}{\int f(p_z) dp_z}. \tag{14}$$

Apparently $\langle p_z \rangle$ stands for the photon linear momentum that has been transferred to the photoelectrons. The nondipole effect we mainly focus on in the present work is the transfer law of the photon linear momentum to the electron in the two-photon ionization process, i.e., the relationship between $\langle p_z \rangle$ and the photon energy ω_0 when ω_0 is varied.

III. RESULTS AND DISCUSSIONS

In this section, we will first validate the reliability of our second-order PT method by comparing its results with those calculated from the nondipole TDSE method [43,56,63,64]. For the hydrogen atomic system, we carry out calculations for laser pulses at different central frequencies $\omega_0 \in [0.28, 0.48]$ a.u. and with different numbers of cycles from $N = 5$ to $N = 100$. The laser intensity is fixed at 1×10^{12} W/cm^2.

After the verification of the validity for the present PT beyond the dipole approximation, we then apply it to the long pulse cases with a nonresonant frequency ω_0 varying from 0.39 to 0.42 a.u. In particular, we will investigate the transfer law of the photon linear momentum in this wavelength region, where a minimum was identified in our previous work [56]. In fact, one will see that the minimum lies between two adjacent resonant peaks in the total ionization probability.

Through a careful analysis of the perturbation theory, we find that the oscillation behavior comes from the interferences between the dipole transition paths and the nondipole transition paths. In the case of linear polarization, two types of dipole pathways participate in such interferences and jointly produce the minimum in the transferred momentum, each of which makes up a different share varying with the incident photon energy. On the contrary, for the case of the circular polarization, only one type of dipole transition channel contributes to the momentum transfer, which shows a monotonic change with the increase of the photon energy and no dichroism is found in the left- and the right-circularly polarized light.

A. Performance of the PT method

We first examine the performance of the second-order PT method by comparing different physical quantities that can be extracted from the full differential distribution of the ionized electron $P(\mathbf{p})$, given by Eq. (12). Specifically, we compute the photoelectron energy distribution

$$P(E) = \iint P(\mathbf{p}) |\mathbf{p}| \sin\theta \, d\theta \, d\phi, \tag{15}$$

the angular distribution

$$P(\theta) = \iint P(\mathbf{p}) |\mathbf{p}|^2 \, dp \, d\phi, \tag{16}$$

and the total ionization probability

$$P_t = \iiint P(\mathbf{p}) |\mathbf{p}|^2 \sin\theta \, dp \, d\theta \, d\phi. \tag{17}$$

To check the accuracy of the second-order PT method in accounting for the nondipole effects, one can extract the difference in the electron angular distribution between the results from the nondipole and dipole description of the interaction Hamiltonian, which is denoted by

$$\Delta P_{nd}(\theta) = P_{nd}(\theta) - P_d(\theta). \tag{18}$$

The above-defined quantities from the PT method can be directly compared with those which can be accurately evaluated from the numerical solution [56] to the TDSE, given in Eq. (1).

In Fig. 1(a), we compare the photoelectron energy distributions from the PT method and the TDSE for lasers at a fixed central frequency of 0.28 a.u. with four different numbers of cycles N. Excellent agreements are achieved for the two-photon ionization in all cases from an ultrashort few-cycle laser pulse with a duration about 0.87 fs ($N = 5$) to a very long laser pulse with a duration about 20 fs ($N = 100$), where a sharp two-photon-ionization peak is clearly seen.

Because the transfer of the photon linear momentum to the electron results from the nondipole effects, one expects

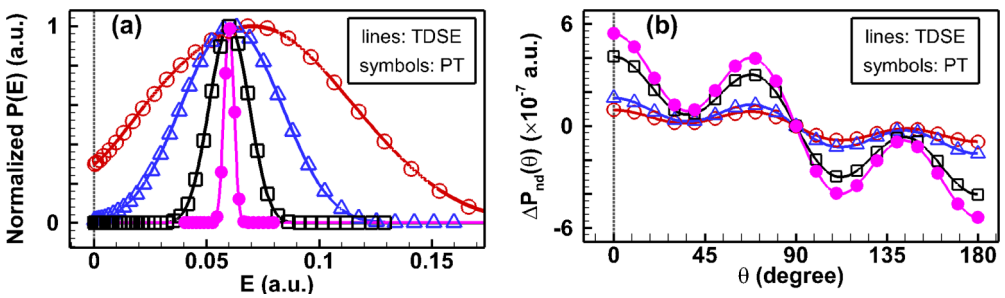

FIG. 1. (a) Photoelectron energy distribution $P(E)$ and (b) angular distribution $\Delta P_{nd}(\theta)$ from the hydrogen ground state exposed to a linearly polarized $\cos^2$-shaped pulse with $\omega_0 = 0.28$ a.u. at various pulse durations: $N = 5$ (the red open circles for the PT), $N = 10$ (the blue triangles for PT), $N = 25$ (the black open squares for the PT), $N = 100$ (the purple solid circles for the PT). In both (a) and (b), solid lines represent the TDSE results. In (a), results for different pulse durations are normalized for a better visibility. In (b), the results for $N = 5$, $N = 10$, and $N = 25$ have been multiplied by a factor 3 for clarity.

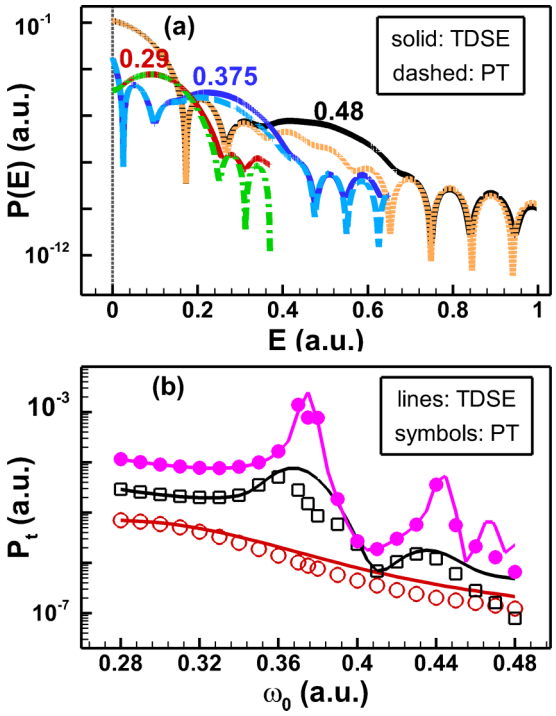

FIG. 2. (a) Photoelectron energy distribution $P(E)$ for the hydrogen $1s$ state exposed to a linearly polarized $\cos^2$-shaped pulse with $N = 5$ at three different ω_0: 0.29 (the green dash-dotted line for PT), 0.375 a.u. (the light blue dashed line for PT), and 0.48 a.u. (the orange dotted line for PT). The solid curves are from the TDSE. (b) Total ionization probabilities at various ω_0 for different pulse durations: $N = 5$ (the red open circles for PT), $N = 25$ (the black open squares for PT), and $N = 100$ (the purple solid circles for PT). Solid lines represent the TDSE results.

a significant difference $\Delta P_{nd}(\theta)$ will occur in the direction of the laser propagation due to the radiation pressure of the laser. That is to say, the nondipole effects can be observed in the electron angular distribution. In Fig. 1(b), we compare $\Delta P_{nd}(\theta)$ calculated by the PT method and the TDSE for the four different pulse durations. Indeed, we see that the transfer of the photon linear momentum does increase the probabilities of photoelectrons along the positive propagation direction [i.e., $\Delta P_{nd}(\theta) > 0$], which corresponds to $p_z > 0$ for photoelectrons ejected at $\theta \in [0^\circ, 90^\circ]$ in Fig. 1(b). On the other hand, the probabilities of photoelectrons with $p_z < 0$ decrease and so $\Delta P_{nd}(\theta)$ is negative for $\theta \in [90^\circ, 180^\circ]$. From Fig. 1(b), one can conclude that the present PT is able to accurately describe the nondipole effects.

From the above discussions, the results from our PT method have shown perfect agreements with those from the TDSE for both short and long pulses. However, it must be pointed out that inaccuracy may occur for the second-order PT method when a significant resonant frequency component is contained in the Fourier spectrum of the incident laser pulse. To see this shortcoming, we compute the photoelectron energy distribution $P(E)$ for $N = 5$ at three different central frequencies $\omega_0 = 0.29$, 0.375, and 0.48 a.u. The results from the PT method and the TDSE are shown in Fig. 2(a). For 0.29 a.u., the agreement of the results from both methods is perfect. For the other two photon energies, obvious differences are observed between the PT method and the TDSE when the photon energy is equal to the resonance frequencies of the hydrogen atomic system.

The deviations can be attributed to the inadequacy of the present PT model in dealing with the resonant case, e.g., $\omega_0 = 0.375$ a.u. At the laser intensity of 1×10^{12} W/cm^2 and the resonance frequency $\omega_0 = 0.375$ a.u., one can estimate the Rabi frequency between the initial $1s$ state and the intermediate $2p$ state to be about 1.75×10^{-3} a.u., which is much larger than the spontaneous decay width of the $2p$ state. In this situation, the Rabi oscillation does occur and the strong coupling between the $1s$ state and the $2p$ state must be considered. Therefore, if the laser frequency is close to a resonance frequency, the mixing of the wave function of the initial state and the intermediate state becomes important in the PT model. However, due to the absence of the strong coupling between the two states, the current PT method is inadequate in quantitatively treating the case where a resonance frequency plays an important role in the laser spectrum. One can also demonstrate this point through the total ionization probability by varying the central frequency for three different pulse durations, as shown in Fig. 2(b); the deviations between the PT and TDSE results become obvious for all cases when the central frequency ω_0 is close to a resonance frequency such as 0.375 a.u.

Nevertheless, for a domain of the central frequency ω_0 between the two adjacent resonance frequencies 0.375 a.u. and 4/9 ($\approx$0.444) a.u., the results from the second-order PT method beyond the dipole approximation agree perfectly with those from the TDSE for the long pulse about 20 fs, as seen in Fig. 2(b) for $N = 100$. In the following section, we will constrain ourselves to this central frequency region for a long pulse of $N = 100$ to analyze the dips of the photoelectron momentum shift $\langle p_z \rangle$ along the laser-propagation direction due to the linear-momentum transfer.

B. Dips in the linear momentum transfer

During the one-photon ionization process, the transfer law of the photon linear momentum is that $\langle p_z \rangle$ will linearly increase with the photon energy in the case of a long pulse [54–56]. It is interesting that for two-photon ionization the TDSE results indicate a different transfer law for circular and linear polarization [56].

In this section, we will turn to analyzing the underlying mechanism of the dips in the electron momentum $\langle p_z \rangle$ along the laser propagation, when the photon energy ω_0 is increased for a linearly polarized pulse. In the previous work [56], we identified a series of minima for the two-photon ionization process. In fact, we found that the minima are located between two adjacent resonant peaks of two-photon ionization, as can be seen from Figs. 3(a) and 3(c) for the hydrogen $1s$ state. We emphasize that this phenomenon also exists for other atomic species, e.g., a series of dips appear in Fig. 3(b) for He described by a model potential in the single active electron approximation [30], in which case the atomic potential in Eq. (2) is given by $V(r) = -\frac{1}{r}[1 + (1 + \beta r/2)e^{-\beta r}]$ with $\beta = 27/8$. These minima are also located between the resonance

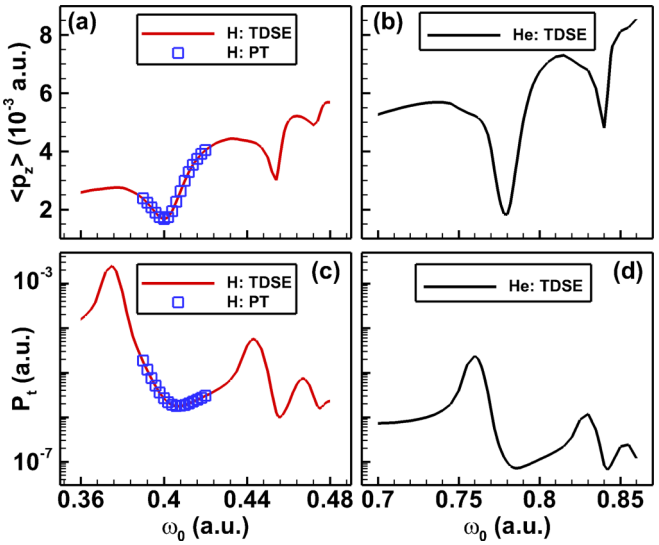

FIG. 3. Expectation of the linear momentum transferred to the photoelectron ionized from (a) the hydrogen and (b) the helium atomic system. The two-photon ionization probability is shown as a function of the central frequency ω_0 for (c) the hydrogen and (d) the helium atomic systems. The square symbols in (a) and (c) are results from the PT method.

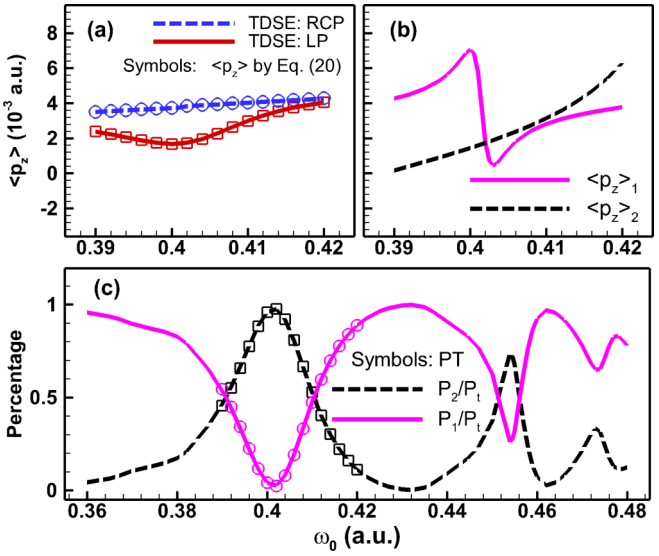

FIG. 4. (a) Photoelectron momentum shift $\langle p_z\rangle$ varies with the photon energy of a pulse with the linear polarization (LP) or the right-handed circular polarization (RCP). The red solid (blue dashed) lines are for the TDSE results of the LP (RCP). The red open squares (blue open circles) represent $\langle p_z\rangle$ of the LP (RCP) obtained by Eq. (20) in the PT method. (b) $\langle p_z\rangle_{1,2}$ of the LP from PT. (c) Purple solid (black dashed) line indicates the TDSE results of P_1/P_t (P_2/P_t) with the symbols from the PT results.

peaks of two-photon ionization of He, as can be seen from Fig. 3(d). The first dip in He is located around $\omega_0 = 0.78$ a.u.

To seek the underlying physics, let us focus on analyzing the first dip for H, i.e., the one located around $\omega_0 = 0.4$ a.u. between the resonant frequencies 0.375 and 0.444 a.u. for the hydrogen atom. In this region, the current PT method works perfectly and is able to produce identical results with those from the TDSE for both $\langle p_z\rangle$ and the total ionization probability, as clearly seen in Figs. 3(a) and 3(c).

According to the selection rules under the dipole approximation, one can classify the transition channels (TC) into two categories, the TC_1^d and the TC_2^d. One of them, the TC_1^d, represents the transition pathways from the ground state first to the intermediate states (p states with the angular quantum number $l = 1$) and then to the d states ($l = 2$). The other one, the TC_2^d type of channels, starts from the ground state to the intermediate states (p states) and ends up with the s states ($l = 0$). With the lowest-order nondipole corrections considered in the interaction Hamiltonian, relevant nondipole transition channels will appear and interfere with the dipole transition channels TC_1^d and TC_2^d. We use TC^{nd} to represent the transition paths involved with the nondipole correction $\frac{z}{c}\mathbf{p}\cdot\mathbf{E}(t) + \frac{z}{c}\mathbf{A}(t)\cdot\mathbf{E}(t)$ in Eq. (3). Please note that although the lowest-order nondipole correction in Eq. (3) and the expression of Eq. (8) depend on the choice of the particular gauge [57], we find that the observable quantities calculated by different gauges agree with each other. For example, a different gauge has been recently adopted in discussing the nondipole effects in molecular ionization [57].

The amplitudes of the nondipole transition channels, $A_{\mathrm{TC}^{nd}}$, are on the order of $O(1/c)$ compared to the amplitudes $A_{\mathrm{TC}_1^d}$ and $A_{\mathrm{TC}_2^d}$ of the dipole channels. According to the nondipole corrections to the Hamiltonian in Eqs. (3) and (8), the probability of a photoelectron ionized with a final momentum $\mathbf{p}$ can be expressed as

$$|A_2|^2 = \left|A_{\mathrm{TC}_1^d} + A_{\mathrm{TC}_2^d}\right|^2 + 2\mathrm{Re}\left(A_{\mathrm{TC}_1^d}A^*_{\mathrm{TC}^{nd}} + A_{\mathrm{TC}_2^d}A^*_{\mathrm{TC}^{nd}}\right). \quad (19)$$

Therefore, the nondipole parts in the electron spectrum come from the interference between the dipole pathways and the nondipole ones, such as $A_{\mathrm{TC}_1^d}A^*_{\mathrm{TC}^{nd}}$ in Eq. (19). These interference terms are on the order of $O(1/c)$ and higher-order terms can be neglected under the laser parameters considered in the present work. Thus the nondipole effect, which induces the nonzero photoelectron momentum shift $\langle p_z\rangle$ along the laser-propagation direction, can be attributed to the interferences between the dipole transition paths and the nondipole transition paths.

Through the current second-order PT method beyond the dipole approximation, one can further explore the origin of the difference in the transfer law for the photon linear momentum for the two-photon ionization by a linearly and a circularly polarized pulse. As can be seen from Fig. 4(a), there is an obvious minimum in the $\langle p_z\rangle$ for the case of the linear polarization, compared against the purely linear relationship for the right-handed circular polarization case. From Eqs. (14) and (19), one can deduce that each interference term in Eq. (19) will contribute a part of the nonzero momentum shift (marked as $\langle p_z\rangle_{1,2}$ in sequence) and $\langle p_z\rangle$ is a summation of these contributions with its own proportion, as can be

expressed as

$$\langle p_z\rangle = \left(\frac{P_1}{P_t}\right)\langle p_z\rangle_1 + \left(\frac{P_2}{P_t}\right)\langle p_z\rangle_2, \tag{20}$$

where $\langle p_z\rangle_{1,2}$ is obtained by assuming only one type of the dipole transition channels and the nondipole ones are involved in the PT method. For instance, $\langle p_z\rangle_1$ is obtained by supposing $|A_2|^2$ to be $|A_{\mathrm{TC}_1^d}|^2 + 2\mathrm{Re}(A_{\mathrm{TC}_1^d}A^*_{\mathrm{TC}^{nd}})$, with a corresponding ionization probability P_1. In Fig. 4(b), it is interesting to notice that $\langle p_z\rangle_1$ behaves in the manner of a Fano profile by scanning the laser central frequency ω_0 while $\langle p_z\rangle_2$ increases almost linearly with the increase of ω_0.

Actually under this hypothesis, it is a good approximation that $P_1 \approx |A_{\mathrm{TC}_1^d}|^2$ and $P_2 \approx |A_{\mathrm{TC}_2^d}|^2$, so $P_1 + P_2 \approx P_t$ due to the relatively small contributions from the nondipole terms. The two dipole transition paths compete with each other and the oscillation patterns of their ratios in Fig. 4(c) lead to the series of minima observed in Fig. 3(a). The momentum shift caused by each interference in Fig. 4(b) and the oscillatory ratio of each dipole pathway in Fig. 4(c) jointly determine the position of the minimum. In the circular polarization case, there will be $P_1/P_t \approx 1$ and $P_2/P_t = 0$ according to the selection rule, thus leading to $\langle p_z\rangle \approx \langle p_z\rangle_1$. Meanwhile, the behavior of $\langle p_z\rangle_1$ by a circularly polarized pulse changes to be a linear relationship with the increase of ω_0, not the Fano profile. Besides, we have discovered no dichroism in the left- and right-circularly polarized light in terms of the linear-momentum-transfer law. In Fig. 4(a), the $\langle p_z\rangle$ of the circular and linear polarization calculated by Eq. (20) through the PT method agree exactly with the TDSE results, which supports our speculation above.

In the case of two-photon single ionization of helium, similar dips of the photoelectron momentum shift $\langle p_z\rangle$ also appear in the case of the linear polarization, as have been seen in Fig. 3(b). One can deduce that the $\langle p_z\rangle$ minima for helium are also determined by the same reasons as for hydrogen discussed above. We notice that the oscillatory pattern of the ratio of each dipole transition pathway in helium has been recently observed from a different perspective [34].

IV. CONCLUSIONS

We have analyzed the nondipole effects in the two-photon ionization process through the second-order time-dependent perturbation theory beyond the dipole approximation. The general good performance of the PT method has been discussed in a number of physical quantities and excellent agreements with the accurate TDSE results have been achieved. However, deviations do appear when the laser spectra have significant components resonant with an intermediate state. The limitation comes from the inadequacy of the present PT model in dealing with the resonant case where the strong coupling between the two states must be properly accounted for.

By using the PT method in the nonresonant regime of two-photon ionization, we identified the physical origins in the different transfer law of photon linear momentum for the case of linearly and circularly polarized pulses. The dips observed in the linear polarization case are jointly caused by interferences between the dipole and nondipole transition pathways and by the oscillation behavior of the proportion of each dipole pathway.

ACKNOWLEDGMENTS

This work is partially supported by the National Natural Science Foundation of China (NSFC) under Grants No. 11725416 and No. 11574010, and by the National Key R&D Program of China (Grant No. 2018YFA0306302). L.Y.P. acknowledges the support by the National Science Fund for Distinguished Young Scholars.

[1] P. Emma *et al.*, Nat. Photon. **4**, 641 (2010).
[2] B. W. J. McNeil and N. R. Thompson, Nat. Photon. **4**, 814 (2010).
[3] T. Ishikawa *et al.*, Nat. Photon. **6**, 540 (2012).
[4] L. Young *et al.*, J. Phys. B **51**, 032003 (2018).
[5] E. Karule, J. Phys. B **4**, L67 (1971).
[6] N. B. Delone, Sov. Phys. Usp. **18**, 169 (1975).
[7] P. Lambropoulos, G. Doolen, and S. P. Rountree, Phys. Rev. Lett. **34**, 636 (1975).
[8] G. Laplanche, A. Durrieu, Y. Flank, M. Jaouen, and A. Rachman, J. Phys. B **9**, 1263 (1976).
[9] R. S. D. Sihombing, M. Katsuragawa, G. Z. Zhang, and K. Hakuta, Phys. Rev. A **54**, 1551 (1996).
[10] A. A. Sorokin, S. V. Bobashev, T. Feigl, K. Tiedtke, H. Wabnitz, and M. Richter, Phys. Rev. Lett. **99**, 213002 (2007).
[11] M. G. Makris, P. Lambropoulos, and A. Mihelič, Phys. Rev. Lett. **102**, 033002 (2009).
[12] M. Dondera, Phys. Rev. A **82**, 053419 (2010).
[13] W. Zernik, Phys. Rev. **135**, A51 (1964).
[14] P. Lambropoulos, Phys. Rev. A **9**, 1992 (1974).
[15] P. Koval, S. Fritzsche, and A. Surzhykov, J. Phys. B **36**, 873 (2003).
[16] F. Lépine, S. Zamith, A. de Snaijer, C. Bordas, and M. J. J. Vrakking, Phys. Rev. Lett. **93**, 233003 (2004).
[17] A. N. Grum-Grzhimailo, E. V. Gryzlova, E. I. Staroselskaya, J. Venzke, and K. Bartschat, Phys. Rev. A **91**, 063418 (2015).
[18] W. Zernik and R. W. Klopfenstein, J. Math. Phys. **6**, 262 (1965).
[19] E. Karule, J. Phys. B **11**, 441 (1978).
[20] E. Karule, J. Phys. B **18**, 2207 (1985).
[21] E. Karule and B. Moine, J. Phys. B **36**, 1963 (2003).
[22] H. R. Varma, M. F. Ciappina, N. Rohringer, and R. Santra, Phys. Rev. A **80**, 053424 (2009).
[23] L. W. Pi and A. F. Starace, Phys. Rev. A **82**, 053414 (2010).
[24] V. Florescu, O. Budriga, and H. Bachau, Phys. Rev. A **84**, 033425 (2011).
[25] V. Florescu, O. Budriga, and H. Bachau, Phys. Rev. A **86**, 033413 (2012).
[26] J. Hofbrucker, A. V. Volotka, and S. Fritzsche, Phys. Rev. A **96**, 013409 (2017).

[27] E. Foumouo, P. Antoine, H. Bachau, and B. Piraux, New J. Phys. **10**, 025017 (2008).
[28] H. Bachau, Phys. Rev. A **83**, 033403 (2011).
[29] K. Stefańska, F. Reynal, and H. Bachau, Phys. Rev. A **85**, 053405 (2012).
[30] L.-Y. Peng and A. F. Starace, Phys. Rev. A **76**, 043401 (2007).
[31] E. A. Pronin, A. F. Starace, M. V. Frolov, and N. L. Manakov, Phys. Rev. A **80**, 063403 (2009).
[32] E. A. Pronin, A. F. Starace, and L.-Y. Peng, Phys. Rev. A **84**, 013417 (2011).
[33] N. L. Manakov, M. V. Frolov, B. Borca, and A. F. Starace, J. Phys. B **36**, R49 (2003).
[34] J. Hofbrucker, A. V. Volotka, and S. Fritzsche, Phys. Rev. Lett. **121**, 053401 (2018).
[35] N. J. Kylstra, R. M. Potvliege, and C. J. Joachain, J. Phys. B **34**, L55 (2001).
[36] M. Førre and A. S. Simonsen, Phys. Rev. A **90**, 053411 (2014).
[37] D. Cricchio, E. Fiordilino, and K. Z. Hatsagortsyan, Phys. Rev. A **92**, 023408 (2015).
[38] M. W. Walser, C. H. Keitel, A. Scrinzi, and T. Brabec, Phys. Rev. Lett. **85**, 5082 (2000).
[39] N. J. Kylstra, R. A. Worthington, A. Patel, P. L. Knight, J. R. Vázquez de Aldana, and L. Roso, Phys. Rev. Lett. **85**, 1835 (2000).
[40] M. Førre, S. Selstø, J. P. Hansen, and L. B. Madsen, Phys. Rev. Lett. **95**, 043601 (2005).
[41] A. Y. Istomin, N. L. Manakov, A. V. Meremianin, and A. F. Starace, Phys. Rev. Lett. **92**, 063002 (2004).
[42] S. Grundmann, F. Trinter, A. W. Bray, S. Eckart, J. Rist, G. Kastirke, D. Metz, S. Klumpp, J. Viefhaus, L. P. H. Schmidt, J. B. Williams, R. Dörner, T. Jahnke, M. S. Schöffler, and A. S. Kheifets, Phys. Rev. Lett. **121**, 173003 (2018).
[43] M.-X. Wang, H. Liang, X.-R. Xiao, S.-G. Chen, W.-C. Jiang, and L.-Y. Peng, Phys. Rev. A **98**, 023412 (2018).
[44] M. Førre, J. P. Hansen, L. Kocbach, S. Selstø, and L. B. Madsen, Phys. Rev. Lett. **97**, 043601 (2006).
[45] O. Hemmers, R. Guillemin, E. P. Kanter, B. Krässig, D. W. Lindle, S. H. Southworth, R. Wehlitz, J. Baker, A. Hudson, M. Lotrakul, D. Rolles, W. C. Stolte, I. C. Tran, A. Wolska, S. W. Yu, M. Y. Amusia, K. T. Cheng, L. V. Chernysheva, W. R. Johnson, and S. T. Manson, Phys. Rev. Lett. **91**, 053002 (2003).
[46] O. Hemmers, R. Guillemin, D. Rolles, A. Wolska, D. W. Lindle, E. P. Kanter, B. Krässig, S. H. Southworth, R. Wehlitz, B. Zimmermann, V. McKoy, and P. W. Langhoff, Phys. Rev. Lett. **97**, 103006 (2006).
[47] T. Khalil, B. Schmidtke, M. Drescher, N. Müller, and U. Heinzmann, Phys. Rev. Lett. **89**, 053001 (2002).
[48] H. Bachau, M. Dondera, and V. Florescu, Phys. Rev. Lett. **112**, 073001 (2014).
[49] M. Dondera, V. Florescu, and H. Bachau, Phys. Rev. A **95**, 023417 (2017).
[50] M. J. Seaton, J. Phys. B **29**, 2373 (1996).
[51] C. T. L. Smeenk, L. Arissian, B. Zhou, A. Mysyrowicz, D. M. Villeneuve, A. Staudte, and P. B. Corkum, Phys. Rev. Lett. **106**, 193002 (2011).
[52] M. Klaiber, E. Yakaboylu, H. Bauke, K. Z. Hatsagortsyan, and C. H. Keitel, Phys. Rev. Lett. **110**, 153004 (2013).
[53] A. Ludwig, J. Maurer, B. W. Mayer, C. R. Phillips, L. Gallmann, and U. Keller, Phys. Rev. Lett. **113**, 243001 (2014).
[54] S. Chelkowski, A. D. Bandrauk, and P. B. Corkum, Phys. Rev. Lett. **113**, 263005 (2014).
[55] P.-L. He, D. Lao, and F. He, Phys. Rev. Lett. **118**, 163203 (2017).
[56] M.-X. Wang, X.-R. Xiao, H. Liang, S.-G. Chen, and L.-Y. Peng, Phys. Rev. A **96**, 043414 (2017).
[57] H. Liang, M.-X. Wang, X.-R. Xiao, Q. Gong, and L.-Y. Peng, Phys. Rev. A **98**, 063413 (2018).
[58] A. F. Starace, in *Theory of Atomic Photonionization*, Handbuch der Physik/Encyclopedia of Physics, Vol. 31 (Springer Verlag, Berlin, 1982).
[59] C. Cohen-Tannoudji, J. Dupont-Roc, and G. Grynberg, *Atom-Photon Interactions* (Wiley-VCH Verlag, Weinheim, Germany, 1998).
[60] A. Maquet, V. Véniard, and T. A. Marian, J. Phys. B **31**, 3743 (1998).
[61] A. A. Krylovetsky, N. L. Manakov, and S. I. Marmo, JETP **92**, 37 (2001).
[62] H. Gouraud, IEEE Trans. Comput. **C-20**, 623 (1971).
[63] L.-Y. Peng and A. F. Starace, J. Chem. Phys. **125**, 154311 (2006).
[64] L.-Y. Peng, W.-C. Jiang, J.-W. Geng, W.-H. Xiong, and Q. Gong, Phys. Rep. **575**, 1 (2015).